Environ. Sci. Technol. **2010,** *44,* 1617–1623

Nitrous Oxide Emissions from the Gulf of Mexico Hypoxic Zone

JOHN T. WALKER,*,† CRAIG A. STOW,‡ AND CHRIS GERON†

U.S. EPA, Office of Research and Development, National Risk Management Research Laboratory, Durham, North Carolina 27711, and NOAA Great Lakes Environmental Research Laboratory, Ann Arbor, Michigan 48108

Received July 9, 2009. Revised manuscript received January 14, 2010. Accepted January 15, 2010.

The production of nitrous oxide (N_2O), a potent greenhouse gas, in hypoxic coastal zones remains poorly characterized due to a lack of data, though large nitrogen inputs and deoxygenation typical of these systems create the potential for large N_2O emissions. We report the first N_2O emission measurements from the Gulf of Mexico Hypoxic Zone (GOMHZ), including an estimate of the emission "pulse" associated with the passage of Tropical Storm Edouard in August, 2008. Prestorm emission rates (25−287 nmol m^{-2} hr^{-1}) and dissolved N_2O concentrations (5 − 30 nmol L^{-1}) were higher than values reported for the Caribbean and western Tropical Atlantic, and on the lower end of the range of observations from deeper coastal hypoxic zones. During the storm, N_2O rich subsurface water was mixed upward, increasing average surface concentrations and emission rates by 23% and 61%, respectively. Approximately 20% of the N_2O within the water column vented to the atmosphere during the storm, equivalent to 13% of the total "hypoxia season" emission. Relationships between N_2O, NO_3^-, and apparent oxygen utilization (AOU) suggest enhanced post storm N_2O production, most likely in response to reoxygenation of the water column and redistribution of organic nitrogen. Our results indicate that mixing related emissions contribute significantly to total seasonal emissions and must therefore be included in emission models and inventories for the GOMHZ and other shallow coastal hypoxic zones.

Introduction

The Gulf of Mexico Hypoxic Zone (GOMHZ), commonly known as the Dead Zone, is an extensive area of recurrent coastal eutrophication (*1*). Seasonal bottom water hypoxia [O_2 < 63 μmol L^{-1} (1)] results from persistent vertical stratification coupled with high surface water productivity driven by nutrients from the Mississippi and Atchafalaya Rivers, which drain the largest watershed in North America (*2*). Hypoxia occurs below the pycnocline nearly continuously from May through September and may extend over 20 000 km^2 (*1*) leading to habitat shifts for a number of upper trophic level species (*1*). Management efforts to reduce hypoxia are focused on reducing nonpoint source nitrogen and phosphorus inputs to streams and rivers draining the Mississippi−Atchafalaya River basin.

* Corresponding author phone: 919-541-2288; fax: 919-541-7885; e-mail: walker.johnt@epa.gov.
† U.S. EPA, Office of Research and Development.
‡ NOAA Great Lakes Environmental Research Laboratory.

Until now, nitrogen research in the GOMHZ has, understandably, focused on characterizing inputs (*3*) and linkages to primary productivity (*1*). Other potentially important aspects of nitrogen biogeochemistry, such as microbial trace gas production, have received less attention (*4*). Of particular interest is the production and emission of nitrous oxide (N_2O), a potent greenhouse gas that is accumulating in the troposphere at a rate of 0.26% yr^{-1} (*5*). Previous studies of N_2O in nutrient impacted and hypoxic coastal zones (*6–10*) show that high productivity, stratification, low O_2, and large N pools typical of these systems produce large emissions. While uncertainties persist in the global N_2O budget (*11*), available data indicate that coastal zones represent a significant fraction (7−61%, ref *12* and references therein) of total oceanic emissions. The contribution of hypoxic zones to total coastal and oceanic emissions remains uncertain due to a lack of data (*8*).

We report the first N_2O emission estimates and water column profile measurements from the GOMHZ collected during the summer of 2008 from aboard the R/V *Pelican*. Our cruise was interrupted by the passage of Tropical Storm Edouard, allowing an opportunity to estimate the emission "pulse" resulting from storm-driven entrainment of N_2O in the middle and bottom of the water column to the surface. Differences in emission rates before and after the storm are characterized as well as relationships between dissolved N_2O, O_2, and nutrient concentrations.

Materials and Methods

We measured dissolved N_2O concentrations using a manual version of the headspace equilibration approach (*13*). Water samples were collected in 5 L Niskin bottles (model 1010; General Oceanics; Miami, FL) attached to a CTD probe and bubble-free subsamples were immediately transferred to a 200 mL flask and sealed without a headspace. Thirty mL was then transferred to a 60 mL syringe to which 30 mL of ultrapure He (Airgas National Welders; Raleigh, NC) was added. The syringe was shaken vigorously for 15 s and allowed to equilibrate before analysis, typically within 30 min to 3 h. Tests indicated that samples were fully equilibrated within 5 min after shaking. A single sample was analyzed from each Niskin bottle and, because samples were processed immediately, the addition of $HgCl_2$ to inhibit microbial activity was not necessary (*13*). The N_2O concentration in the headspace was determined by gas chromatography/electron capture detection. A full description of the analytical system is included as Supporting Information (SI) section S1.

The dissolved N_2O concentration (C_w, nmol L^{-1}) was determined as (*14*):

$$C_w = \left(\beta x P V_w + \frac{xP}{RT} V_{hs}\right) / V_w \quad (1)$$

where β is the Bunsen solubility (nmol L^{-1} atm^{-1}) (*15*), x is the concentration (ppb) of headspace N_2O, P is atmospheric pressure (atm), and V_w and V_{hs} are the volumes of water and headspace, respectively, in the syringe. R is the universal gas constant and T is the temperature at headspace equilibration. Water temperature was measured at the time of sampling and immediately following headspace injection onto the GC and C_w was corrected for the corresponding difference in N_2O solubility (*16*). N_2O % saturations (Sat) were calculated as follows :

$$\text{Sat} = 100 C_w / C_a \quad (2)$$

10.1021/es902058t
Published on Web 02/04/2010

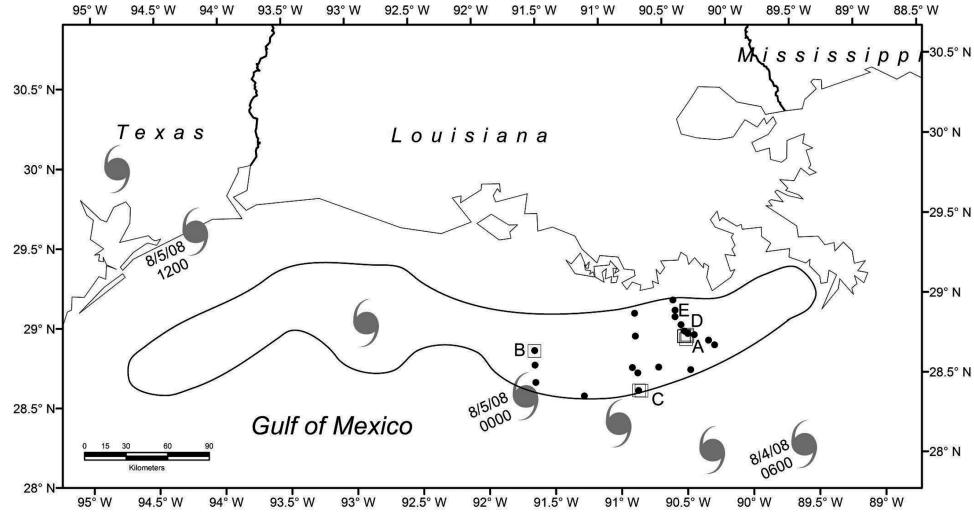

FIGURE 1. Pre- (□, $N = 8$) and poststorm (●, $N = 22$) N_2O sampling locations. The approximate perimeter of the hypoxic zone (black line) and path of Tropical Storm Edouard are also shown. Approximate locations of stations A, B, and C in Figure 2 and A, D, and E in SI Figure S3 are also labeled.

where C_a is the dissolved N_2O concentration in equilibrium with the atmosphere determined from air samples taken 2 m above the water surface. ΔN_2O is defined as $C_w - C_a$. With respect to water samples, "surface" is defined as <1 m depth. Air samples were collected every 1 to 4 h during the collection of water samples. Pre- and poststorm average air concentrations were 321.9 ± 1.5 ppb ($N = 8$) and 322.5 ± 1.9 ppb ($N = 11$), respectively, which are similar to the average concentration (322.1 ± 0.32 ppb) observed at NOAA's northern hemispheric in situ halocarbon monitoring stations (Mauna Loa, Hawaii; Niwot Ridge, Colorado; Pt. Barrow, Alaska; Summit, Greenland) during August, 2008 (*17*). Instrument precision was 0.23% at ambient concentrations.

The N_2O flux (F) to the atmosphere was calculated as (*16*):

$$F = k_w(C_w - C_a) \quad (3)$$

and the gas transfer coefficient k_w (m s^{-1}) was calculated as (*18*):

$$k_w = 9.2510^{-7}U_{10} + 6.1710^{-7}U_{10}^2 \quad (4)$$

where U_{10} is wind speed at 10 m above the water. Shipboard instantaneous (1 sample every 10 s) wind speed measured at z = 17 m (model 05103 wind monitor; R.M. Young Company; Traverse City, MI) was averaged over the hour preceding surface sample collection and adjusted to the reference height $z_r = 10$ m using the power law relationship

$$U(z)/U(z_r) = (z/z_r)^m \quad (5)$$

where the exponent m is taken as 0.1 for coastal waters (*19*). k_w was adjusted by multiplying with $(Sc/600)^{-0.5}$ where Sc is the Schmidt number for N_2O calculated as a function of the kinematic viscosity of seawater (*20*) and the diffusion coefficient of N_2O (*21*). Mean error in the flux calculation (eq 3) is 38.0 ± 5.0% (70.0 ± 40.0 nmol m^{-2} hr^{-1}), which is dominated by the uncertainty in k. Detailed error calculations are described in SI section S2. Ancillary measurements and statistical methods are described in SI sections S3 and S4, respectively.

Results and Discussion

We measured vertical profiles of dissolved N_2O at multiple locations within the GOMHZ between August 2 and 7, 2008 from the R/V *Pelican*. Our survey was interrupted by Tropical Storm Edouard, which traveled northwest across the hypoxic zone, passing approximately 100 km south of the Louisiana coast on August 4 before making landfall along the Texas coast between High Island and Sabine Pass on August 6 (Figure 1). Maximum sustained surface wind speeds ranged from 13 to 28 m s^{-1} (*22*). Although TS Edouard disrupted our planned investigation, it provided an opportunity to estimate the release of N_2O associated with episodic mixing events. We collected 15 conductivity, temperature, and depth (CTD) profiles, along with other water measurements, prior to the passage of Edouard, in depths ranging from 4 to 32 m. Dissolved N_2O was sampled at a subset of eight locations. Sampling was discontinued at 2100 UTC on 8/3/08 in anticipation of TS Edouard, at which time the R/V *Pelican* returned to port in Cocodrie, LA. Sampling resumed at 1400 UTC on 8/5/08, approximately 20 h after the passage of TS Edouard and continued through 0930 UTC on 8/7/08, during which time 27 additional CTD profiles were collected over the same spatial extent of the prestorm sampling domain. Dissolved N_2O was sampled at a subset of 22 locations.

Vertical Profiles. Except for the shallowest cast (4 m), all prestorm vertical profiles showed a strong halocline starting at 2−4 m and one or more hypoxic layers below 6 m. Composite profiles (SI Figure S1) show that, on average, the bottom 20% of the water column was hypoxic. Dissolved N_2O concentrations ranged from 5.0 to 30.0 nmol L^{-1} and exhibited a subsurface maximum concentration in the middle or bottom of the water column coincident with lower O_2 (SI Figure S1). Nutrient profiles were characterized by decreasing dissolved organic nitrogen (DON) from the surface to the bottom, whereas NO_3^- showed the opposite pattern (SI Figure S1). Surface water (<1 m depth) was supersaturated with N_2O (108−133%) at all sampling points (Table 1) and corresponding emission estimates (eq 3) ranged from 25.0 to 287.0 nmol N_2O m^{-2} hr^{-1}. Vertical mixing of some portion of the water column was evident in all of the poststorm profiles (SI Figure S1). Comparing across sites, temperature and salinity profiles indicated mixing to depths between 15 and 20 m. Only 10 of the 27 poststorm profiles showed evidence of hypoxia, which was confined to the bottom few meters and less severe than prestorm. Storm-induced vertical mixing is also evident in the individual poststorm N_2O profiles (Figure 2), which showed a range in concentrations from 7.0 to 47.0 nmol N_2O L^{-1}. N_2O in the middle and lower column was mixed upward, significantly increasing average surface N_2O concentrations and emission fluxes relative to prestorm

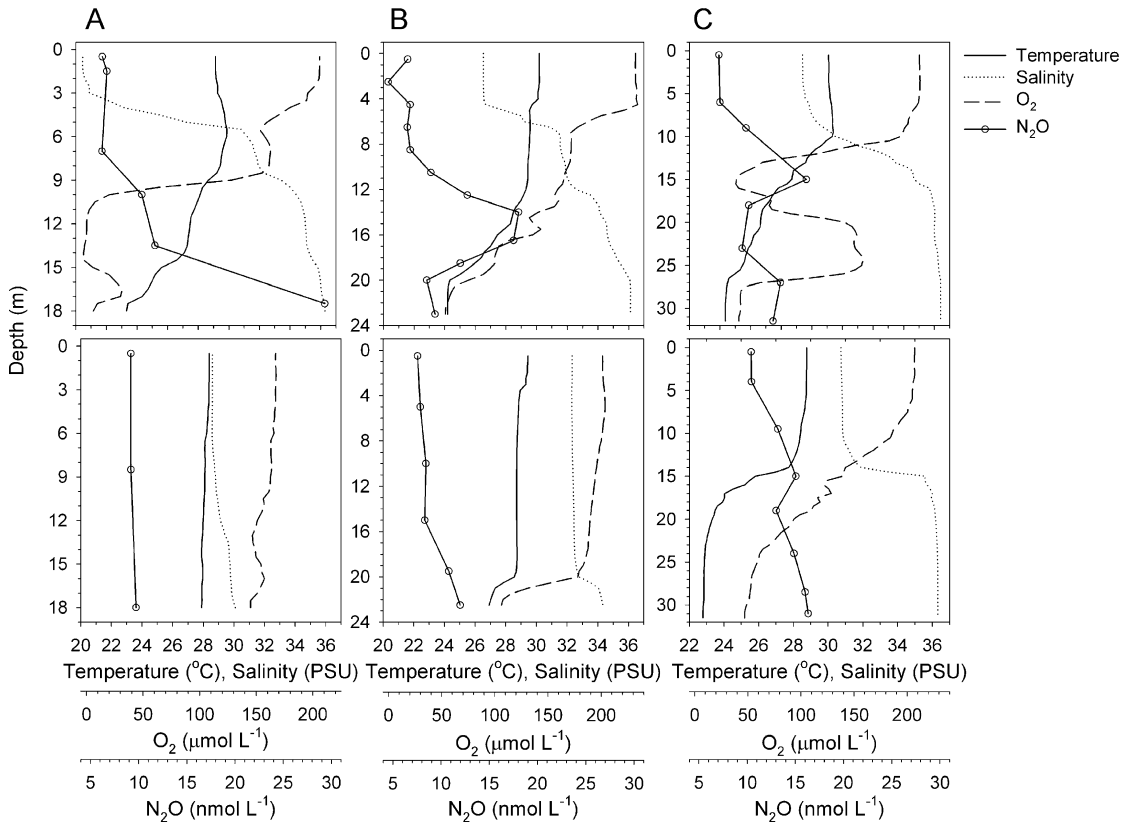

FIGURE 2. Pre- and poststorm temperature, salinity, O_2, and N_2O profiles at locations A, B, and C in Figure 1.

TABLE 1. Pre- (N = 10) and Poststorm (N = 22) Average (±Standard Error) N_2O Concentrations in Air (C_{air}), Surface Water (C_w), % Saturation Relative to the Atmosphere, Wind Speed at 10 m (U_{10}), and Emission Flux. Pre- and Poststorm Differences were Tested Using the Wilcoxon Rank-Sum Test

	C_{air} (ppb)	C_w (nmol L^{-1})	saturation (%)	U_{10} (m s^{-1})	flux (nmol m^{-2} hr^{-1})
prestorm	321.9 ± 1.5	7.26 ±0.13[a]	120.0 ± 2.0[a]	5.5 ± 0.5	136.0 ± 27.0[b]
poststorm	322.5 ± 1.9	8.91 ± 0.30	148.0 ± 5.0	4.8 ± 0.4	219.0 ± 28.0

[a] Pre- and poststorm means significantly different at P = 0.01. [b] Pre- and poststorm means significantly different at P = 0.1.

levels (Table 1). Poststorm N_2O saturation of the surface water ranged from 117 to 195% with corresponding surface emission estimates ranging from 51.0 to 487.0 nmol N_2O m^{-2} hr^{-1}. Note that the difference between pre- and poststorm emissions (Table 1) also reflects the influence of wind speed, which was ≈15% higher, on average, during the prestorm period. The increased surface saturation of N_2O persisted throughout the poststorm sampling period. Similarly, Naik et al. (*23*) observed a doubling of the surface layer N_2O concentration in the Arabian Sea, up to 13 nmol L^{-1}, 4 days after the passage of a moderately intense cyclone, which they attributed to entrainment from the thermocline associated with vertical mixing.

Figure 2 shows example vertical profiles of O_2, salinity, water temperature, and dissolved N_2O at the three stations where a full suite of measurements was taken before and after the storm. The profiles range in depth from 18 to 32 m and cover the spatial extent of the sampling domain. Corresponding profiles of N_2O, NO_3^-, and dissolved organic nitrogen (DON) are included as SI Figure S2. Profile A, taken near the eastern perimeter of the sampling domain, shows a deep layer of hypoxia below 10 m and increasing N_2O to the bottom. The corresponding poststorm profile indicates vertical mixing and reoxygenation of the entire water column. Only 80% of the mass of N_2O in the prestormwater column is accounted for in the poststorm profile, suggesting a loss to the atmosphere equivalent to 45.0 μmol N_2O m^{-2} during the storm. Figure 2B shows a vertical profile from a station on the western boundary of the sampling domain and near the center of the perimeter hypoxic zone. Hypoxia exists below 21 m and the maximum N_2O concentration is observed in the middle of the water column where NO_3^- begins to increase with depth. At this location, the poststorm profile indicates vertical mixing down to approximately 20 m. Ninety percent of the prestorm mass of N_2O is retained in the water column poststorm (85% within the 0−20 m mixed layer), equivalent to an emission of 22.0 μmol N_2O m^{-2}.

The third profile, Figure 2C, was measured at the southern perimeter of the hypoxic zone in deeper water. Here, the salinity and temperature profiles indicate mixing down to approximately 15 m. The O_2 profile, however, suggests some intrusion through, and mixing within, the lower layer. The N_2O profile is also consistent with mixing in both layers though there is a 27% overall increase in the total mass of N_2O in the water column. N_2O concentrations are higher at all depths relative to the prestorm profile, with similar increases in the upper (0−15 m) and lower (15−32 m) layers of 27 and 28%, respectively. Decreasing organic nitrogen and

O_2 concentrations with depth and corresponding increasing NO_3^- is consistent with poststorm N_2O production via nitrification as discussed later.

While the poststorm profiles clearly show evidence of venting during the storm and suggest poststorm N_2O production, variability in the poststorm profiles is also likely influenced to some extent by advection. Though the poststorm profiles are not indicative of widespread advection of more saline water from outside the hypoxic zone, five stations that were sampled twice after the storm, all of which were along the north/south transect including stations A, D, and E in Figure 1, exhibited variability consistent with localized advection. Example profiles are shown in SI Figure S3. The station shown in Figure 2A was sampled on August 2 (prestorm) and August 5 (poststorm), and again on August 7. The August 7 profile (SI Figure S3) shows the reappearance of a different water mass in the lowest meter of the column, which also contained elevated N_2O (23.0 nmol L^{-1}). This feature is suggestive of advection of bottom water that was unmixed or less intensely mixed during the storm. It is notable, though, that N_2O concentrations are ≈25% higher in the well mixed portion of the water column (0.5 and 11.5 m) than at similar depths on August 5. Thus it is difficult to assess the relative importance of advection versus poststorm chemical processing when comparing poststorm profiles separated in time. Profiles in shallower water (SI Figure S3 D and E) along the same transect also show changes in temperature and salinity between August 5 and 7 consistent with advection. Though all of the profiles showed lower oxygen in the lower water column on August 7, it is unclear how much of the change is related to advection versus new deoxygenation. N_2O profiles were not measured at stations D and E prestorm or on August 7. N_2O measurements taken at those stations on August 5 showed well-mixed profiles (observations consisted of surface, middle, and bottom) with concentrations in the range 7.1−7.8 nmol L^{-1}. We may conclude that the poststorm composite N_2O profile (SI Figure S1) reflects the combined effects of vertical mixing, venting to the atmosphere, poststorm new N_2O production, advection, and spatiotemporal variability in the relative importance of these processes. Future studies designed specifically to assess storm impacts would ideally employ a combination of shipboard CTD sampling and fixed location sampling of temperature, salinity, and O_2 over several days to weeks following the storm.

Because some of the poststorm profiles likely contain "new" subsurface N_2O, a conservative estimate of the storm-related emission pulse may be established by comparing the depth-normalized (measurement depth/total depth) average prestorm profile, applied over the maximum observed depth of storm induced mixing (20 m), to a uniform poststorm profile of 8.9 nmol N_2O L^{-1} (Table 1) over the same depth. Note that 8.9 nmol N_2O L^{-1} is the average poststorm concentration at the surface. This approach yields a storm emission pulse of 51.0 μmol N_2O m^{-2} or 22% of total N_2O mass in the prestorm water column. Scaled up to the area of the hypoxic zone [final 2008 area of 20 720 km^2 (*24*)], this is equivalent to 1057 kmol N_2O or 13% of the seasonal emission total (8116 kmol N_2O) in the absence of any storms using our prestorm emission rate as the baseline.

Relationships between N_2O, O_2, and Nutrients. Classification and Regression Tree (CART, see SI section S4 for description) analysis of the data (Figure 3), with N_2O as the response variable and NO_3^- and O_2 as candidate predictors, indicates an initial split at an NO_3^- concentration of 5.6 μmol L^{-1}, with second and third splits at dissolved O_2 concentrations of 39.2 μmol L^{-1} and 166.7 μmol L^{-1}. These partitions,

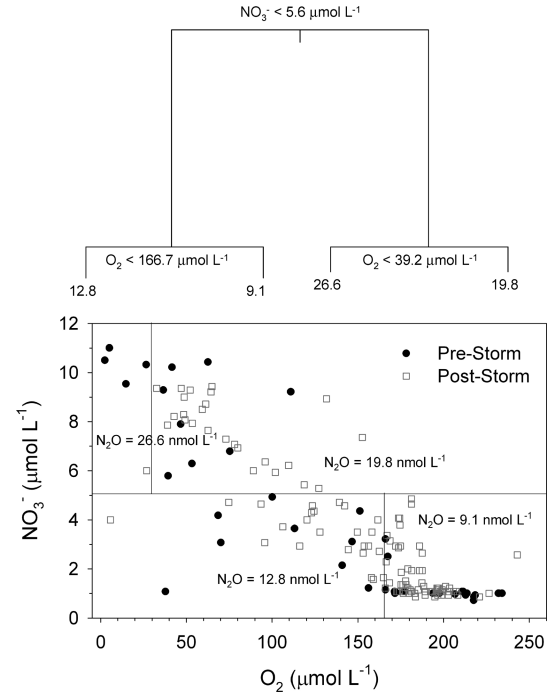

FIGURE 3. Tree and scatterplot display of CART model results.

shown on a plot of NO_3^- vs dissolved O_2 (Figure 3), illustrate that the highest mean N_2O concentrations occurred in hypoxic water near the bottom; conversely, the lowest N_2O concentrations occurred at high O_2 levels with low NO_3^-, which is generally near the surface. The best linear model (R^2 = 0.57, mse = 0.017, N = 154) to predict N_2O from the candidate predictors was

$$\log_{10}(N_2O) = \underset{(0.12)}{1.1} + \underset{(0.14)}{0.56}\beta_1 - \underset{(0.06)}{0.098}\log_{10}(O_2) - \underset{(0.07)}{0.22}\beta_1\log_{10}(O_2) + \underset{(0.04)}{0.23}\log_{10}(NO_3^-) + \varepsilon \quad (6)$$

where β_1 = zero before the storm and one afterward, ε is the model error term and the numbers in parentheses are the standard errors of their respective parameter estimates. Pre- and poststorm intercepts are significantly different (P<0.01), indicating higher average concentrations poststorm. Negative and positive correlations between N_2O and O_2 and NO_3^-, respectively, are also statistically significant (P < 0.01) and pre- (P<0.1) and poststorm (P<0.01) slopes for the O_2 factor are distinctly different.

Our modeling results are consistent with the correlations between N_2O, NO_3^-, and O_2 widely observed in other studies (*25*) and generally attributed to nitrification, the aerobic (i.e., oxygen consuming) oxidation of reduced nitrogen (NH_4^+) to nitrite (NO_2^-) and nitrate (NO_3^-), from which N_2O is produced in trace amounts (*26, 27*). This process begins with the mineralization of organic nitrogen to NH_4^+. The slope of the linear relationship between ΔN_2O and apparent oxygen utilization (AOU) (Figure 4) provides an estimate of the amount of N_2O produced per amount of O_2 consumed (*28*). Pre- and poststorm ΔN_2O/AOU ratios (slopes) were 0.048 nmol μmol^{-1} and 0.096 nmol μmol^{-1}, respectively (Figure 4), which are within the range of values for the open ocean (*25*). Corresponding linear relationships between ΔN_2O and NO_3^- concentration yield slopes ($\Delta N_2O/NO_3^-$), expressed as mol N_2O−N produced per mol NO_3^-−N produced, of 0.07% and 0.13%, respectively.

Higher poststorm ΔN_2O/AOU (Figure 4) and $\Delta N_2O/NO_3^-$ ratios may reflect an enhancement of N_2O production associated with reoxygenation of the water column and

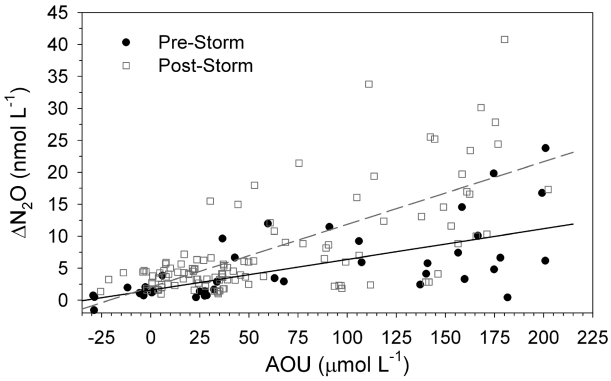

FIGURE 4. Relationships between ΔN_2O (nmol L^{-1}) and AOU (μmol L^{-1}). Prestorm regression equation (solid line) is $y = 1.68 + 0.048x$ ($R^2 = 0.42$); standard errors for the slope and intercept are 0.93 and 0.009, respectively. Poststorm regression equation (dashed line) is $y = 1.98 + 0.096x$ ($R^2 = 0.50$); standard errors for the slope and intercept are 0.71 and 0.009, respectively.

vertical redistribution of organic nitrogen, the substrate for nitrification, that accumulates in the surface layer (i.e., above the halocline, SI Figure S1). The occurrence of the highest concentrations of DON and low NO_3^- near the surface is consistent with inhibition of nitrification in the presence of light (*29*). Vertical mixing of the organic nitrogen pool to depths of sufficient light attenuation would be expected to stimulate nitrification. Mixing would also produce a more uniform distribution of dissolved and particulate forms of organic nitrogen compared to prestorm conditions, thus pre- and poststorm differences in N_2O yields may reflect differences in the C:N ratio of nitrified organic material (*25*). Enhanced N_2O production following reoxygenation of the water column has also been observed in the Arabian (*23*) and Baltic Seas (*30*).

While our results are consistent with N_2O production via nitrification, considerable scatter around the regression lines in Figure 4 and our observations of high organic nitrogen (0.4−45.1 μmol N L^{-1}) and NO_3^- concentrations (0.7−11.0 μmol N L^{-1}) and a large range in O_2 concentrations suggest the possibility that multiple processes may be important. Denitrification, the reduction of NO_3^- to N_2, or coupled nitrification/denitrification in the water column and sediment may be additional sources of N_2O. Oceanic production of N_2O by denitrification is thought to be generally restricted to sediments and low oxygen areas in the tropics and subtropics (ref (*8*) and references therein). N_2O is consumed under suboxic conditions ($O_2 < 4.5$ μmol L^{-1}) by denitrification, whereas denitrifier (and nitrifier) yields can be large (*31, 32*) in the region of transition from suboxic to hypoxic conditions. Though widespread hypoxia was observed in our study, only a single observation (N_2O water sample) was below the suboxic threshold of $O_2 < 4.5$ μmol L^{-1}. Thus the majority of our observations were in the region of deoxygenation where denitrification is expected to be limited. We did not observe any obvious nonlinearity in the relationship between ΔN_2O and AOU that may be indicative of high denitrifier yields in the transition from hypoxia to suboxia. Our results are consistent with Childs et al. (*4*), which examined denitrification potential in surface, midwater, and bottom water within the GOMHZ and found no denitrifier N_2O production. Cumulatively, our results suggest nitrification as the primary source of N_2O in the water column. This pattern is supported by the work of Pakulski et al. (*33*), which examined nutrient cycling processes in the Mississippi and Atchafalaya river plumes and concluded that the high observed rates of NH_4^+ oxidation indicate high rates of water-column nitrification on the inner Louisiana shelf.

In shallow systems such as the GOMHZ, production and consumption of N_2O within the sediment may influence concentrations within the lower water column. Denitrification has been observed in surface sediments within the GOMHZ (*4*), though rates are on the low end of observations from other systems. As noted, only one of our samples contained O_2 below the 4.5 μmol L^{-1} level below which N_2O consumption by denitrification is observed, which suggests that sufficient O_2 was generally present in the surface sediment to support N_2O production via coupled nitrification/denitrification (*31, 32*). Thus, we can not rule out the possibility that N_2O observed in bottom water samples was produced in the sediment, either by denitrification or coupled nitrification/denitrification, or that this contributed to the difference in N_2O concentrations and O_2/NO_3^- relationships observed before and after the storm. More direct examination of nutrient cycling processes (e.g., microbial community structure, nitrification/denitrification rates, and their relation to N pools) is needed to fully characterize the dynamics of N_2O production within the water/sediment system.

Implications

Pre- and poststorm average N_2O emissions are higher than values reported for the Caribbean (*34*) and western tropical Atlantic (*16, 34*). However, average N_2O concentrations (pre- and poststorm) and emissions are on the lower end of the range of observations from other coastal hypoxic systems compiled in a recent review by Naqvi et al. (*8*). The difference may be that the GOMHZ is more physically dynamic than the deeper hypoxic coastal areas previously studied. The GOMHZ is shallower than most of the hypoxic zones discussed by Naqvi et al. (*8*) and therefore prone to more frequent mixing of the entire water column, thereby possibly preventing accumulation of N_2O in the middle and bottom water to levels observed in deeper systems.

Our findings illustrate the necessity of capturing the important scales of temporal variability in field measurements, both steady-state and transient (i.e., mixing) events, from which emission models and inventories are constructed and underscore the need for extensive characterization of dynamic systems such as the GOMHZ. We estimate that the potential emission pulse associated with Tropical Storm Edouard is ≈13% of the seasonal emission total for the GOMHZ in the absence of any storms. Over the past 10 years, an average of 3.6 tropical storms occurred annually in the northeastern (north of 25°/west of −85°) Gulf of Mexico during hypoxia season (*22*). Our data suggest that this number of storms could increase total N_2O emissions from the GOMHZ by ≈50% compared to years without storms. While this estimate is significant, and likely conservative considering the possible effects of lesser meteorological events, the overall importance of mixing related emissions depends on the rate at which N_2O re-establishes following individual events and the extent to which mixing enhances N_2O production rates. Previous observations in the GOMHZ indicate rapid reestablishment of bottom (20 m) hypoxia, within a few days to weeks, following the passage of tropical storms and cold fronts (*1, 2*). While our profiles showed possible new deoxygenation in the middle and lower water column 2 days after the storm, the extent to which the profiles were influenced by advection of water unaffected by the storm is uncertain. However, our results (Figure 4) do indicate poststorm enhancement of N_2O production following mixing-related venting of subsurface N_2O, an observation that is consistent with data from the Arabian and Baltic Seas (*23, 30*). Cumulatively, current evidence suggests that total seasonal N_2O emissions from the GOMHZ should correlate positively with the frequency of mixing events. Alternatively, because the extent of the hypoxic zone is related to the volume and composition of

spring discharge from the Mississippi and Atchafalaya Rivers (*1*), the system may have a limited seasonal capacity for restratification and N_2O production following a succession of strong mixing events. Thus, the net effect on N_2O emissions of these potentially conflicting processes presents several possibilities, inviting further investigation.

Our findings support the emerging view (*35*) that regional and global estimates of aquatic N_2O emissions must include contributions from storm related mixing events in addition to coastal upwelling associated with Ekman transport (*36*). This may be particularly important for shallow hypoxic coastal waters, which experience conditions favorable for high N_2O production rates and are susceptible to complete mixing of the water column. Coastal waters, including estuaries, contribute significantly [0.82 Tg N yr^{-1}, ≈15% (*11*)] to total aquatic emissions even without explicit consideration of storm related emissions. Furthermore, the relative importance of this component of the global budget will increase in the future as coastal hypoxia expands (*37*). The problem may be amplified by climate related increases in precipitation and riverine delivery of nutrients to coastal areas and possible increases in the frequency and intensity of tropical cyclones (i.e., large scale mixing events) (*38, 39*), which have a positive feedback to emissions of N_2O.

Acknowledgments

This work was supported by the U.S. EPA Office of Research and Development and NOAA CSCOR Award NA06NOS4780148. We thank the captain and crew of the R/V *Pelican* (Louisiana Universities Marine Consortium), Bill Preston (U.S. EPA), and Wayne Robarge (North Carolina State University, Department of Soil Science) for field and analytical support. We also thank Mike Roman and Steve Brandt for the opportunity to participate in the 2008 cruise. This manuscript is GLERL contribution number 1544.

Supporting Information Available

Additional information on analytical and statistical methods, flux uncertainty, ancillary data, and figures of vertical profiles are also presented. This material is available free of charge via the Internet at http://pubs.acs.org.

Literature Cited

(1) Rabalais, N. N.; Turner, R. E.; Wiseman, T. J., Jr. Hypoxia in the Gulf of Mexico. *J. Environ. Qual.* **2001**, *30*, 320–329.
(2) Rabalais, N. N.; Turner, R. E.; Sen Gupta, B. K.; Boesch, D. F.; Chapman, P.; Murrell, M. C. Hypoxia in the northern Gulf of Mexico: Does the science support the plan to reduce, mitigate, and control hypoxia. *Estuaries Coasts* **2007**, *30*, 753–772.
(3) Goolsby, D. A.; Battaglin, W. A.; Aulenbach, B. T.; Hooper, R. P. Nitrogen input to the Gulf of Mexico. *J. Environ. Qual.* **2001**, *30*, 329–336.
(4) Childs, C. R.; Rabalais, N. N.; Turner, R. E.; Proctor, L. M. Sediment denitrification in the Gulf of Mexico zone of hypoxia. *Mar. Ecol.: Prog. Ser.* **2002**, *240*, 285–290.
(5) Forster, P. ; et al. Changes in atmospheric constituents and in radiative forcing. In *Climate Change 2007: The Physical Science Basis. Contribution of Working Group I to the Fourth Assessment Report of the Intergovernmental Panel on Climate Change*; Solomon, S. ; et al. Eds; Cambridge University Press: New York; 2007; pp 129−234.
(6) Kroeze, C.; Seitzinger, S. P. Nitrogen inputs to rivers, estuaries and continental shelves and related nitrous oxide emissions in 1990 and 2050: A global model. *Nutr. Cycling Agroecosyst.* **1998**, *52*, 195–212.
(7) Codispoti, L. A.; Elkins, J. W.; Yoshinari, T.; Friedrich, G. E.; Sakamoto, C. M.; Packard, T. T. On the nitrous oxide flux from productive regions that contain low oxygen waters. In *Proceedings of the International Symposium on the Indian Ocean*, New Delhi, India, 1992.
(8) Naqvi, S. W. A.; Bange, H. W.; Farıas, L.; Monteiro, P. M. S.; Scranton, M. I.; Zhang, J. Coastal hypoxia/anoxia as a source of CH_4 and N_2O. *Biogeosciences Discuss.* **2009**, *6*, 9455–9523.
(9) Bange, H. W.; Rapsomanikis, S.; Andreae, M. O. Nitrous oxide in coastal waters. *Global Biogeochem. Cycles* **1996**, *10*, 197–207.
(10) Naqvi, S. W. A.; et al. Increased marine production of N_2O due to intensifying anoxia on the Indian continental shelf. *Nature* **2000**, *408*, 346–349.
(11) Seitzinger, S. P.; Kroeze, C.; Styles, R. V. Global distribution of N_2O emissions from aquatic systems: natural emissions and anthropogenic effects. *Chemosphere: Global Change Sci.* **2000**, *2*, 267–279.
(12) Bange, H. W. New directions: The importance of oceanic nitrous oxide emissions. *Atmos. Environ.* **2006**, *40*, 198–199.
(13) Elkins, J. W. Determination of dissolved nitrous oxide in aquatic systems by gas chromatography using electron-capture detection and multiple phase equilibration. *Anal. Chem.* **1980**, *52*, 263–267.
(14) Walter, S.; Peeken, I.; Lochte, K.; Webb, A.; Bange, H. W. Nitrous oxide measurements during EIFEX, the European Iron Fertilization Experiment in the subpolar South Atlantic Ocean *Geophys. Res. Lett.* **2005**, *32*, DOI: 10.1029/2005GL024619.
(15) Weiss, R. F.; Price, B. F. Nitrous oxide solubility in water and seawater. *Mar. Chem.* **1980**, *8*, 347–359.
(16) Walter, S.; Bange, H. W.; Wallace, D. W. R. Nitrous oxide in the surface layer of the tropical North Atlantic Ocean along a west to east transect. *Geophys. Res. Lett.* **2004**, *31*, DOI: 10.1029/2004GL019937.
(17) NOAA. Nitrous oxide data from the NOAA/ESRL halocarbons in situ program. ftp: //ftp.cmdl.noaa.gov/hats/n2o/insituGCs/CATS/ (2008).
(18) Nightingale, P.; Malin, G.; Law, C. S.; Watson, A. J.; Liss, P. S.; Liddicoat, M. I.; Bouting, J.; Upstill-Goddard, R. C. In situ evaluation of air-sea gas exchange parameterizations using novel conservative and volatile tracers. *Global Biogeochem. Cycles* **2000**, *4*, 373.
(19) Arya, P. *Introduction to Micrometeorology*; Academic Press, Inc.: San Diego, CA; 1988.
(20) Siedler, G.; Peters, H. Properties of seawater In *Oceanography*; Sündermann, J. Ed.; Springer Verlag: New York; 1986, pp 233−264.
(21) Rhee, T. S. PhD thesis. Texas A&M University, College Station, TX, 2000.
(22) NOAA National Hurricane Center. Season Archive. http://www.nhc.noaa.gov/pastall.shtml (2008).
(23) Naik, H.; Naqvi, S. W. A.; Suresh, T.; Narvekar, P. V. Impact of a tropical cyclone on biogeochemistry of the central Arabian Sea *Global Biogeochem. Cycles* **2008**, *22*, DOI: 10.1029/2007GB003028.
(24) Louisiana Universities Marine Consortium (LUMCON) Press release. July 28, 2008. http://www.gulfhypoxia.net/research/shelfwidecruises/2008/PressRelease08.pdf.
(25) Nevison, C. D.; Butler, J. H.; Elkins, J. W. Global distribution of N_2O and the delta N_2O-AOU yield in the subsurface ocean. *Global Biogeochem. Cycles* **2003**, *17*, DOI: 10.1029/2003GB002068.
(26) Elkins, J. W.; Wofsy, S. C.; McElroy, M. B.; Kolb, C. E.; Kaplan, W. A. Aquatic sources and sinks for nitrous oxide. *Nature* **1978**, *275*, 602–606.
(27) Yoshinari, T. Nitrous oxide in the sea. *Mar. Chem.* **1976**, *4*, 189–202.
(28) Bange, H. W. Gaseous nitrogen compounds (NO, N_2O, N_2, NH_3) in the ocean. In *Nitrogen in the Marine Environment*; Capone, D. G., et al., Eds.; Elsevier: Amsterdam, 2008.
(29) Horrigan, S. G.; Carlucci, A. F.; Williams, P. M. Light inhibition of nitrification in sea-surface films. *J. Mar. Res.* **1981**, *39*, 557–565.
(30) Schweiger, B.; Hansen, H. P.; Bange, H. W.; A time series of hydroxylamine (NH_2OH) in the southwestern Baltic Sea *Geophys. Res. Lett.* **2007**, *34*, DOI: 10.1029/2007GL031086.
(31) Joergensen, K. S.; Jensen, H. B.; Soerensen, J. Nitrous oxide production from nitrification and denitrification in marine sediment at low oxygen concentrations. *Can. J. Microbiol.* **1984**, *30*, 1073–1078.
(32) Goreau, T. J.; Kaplan, W. A.; Wofsy, S. C.; McElroy, M. B.; Valois, F. W.; Watson, S. W. Production of NO_2^- and N_2O by nitrifying bacteria at reduced concentrations of oxygen. *Appl. Environ, Microbiol.* **1980**, *40*, 526–532.
(33) Pakulski, J. D.; Benner, R.; Whitledge, T.; Amon, R.; Eadie, B.; Cifuentes, L.; Ammerman, J.; Stockwell, D. Microbial metabolism and nutrient cycling in the Mississippi and Atchafalaya River plumes. *Estuarine Coastal Shelf Sci.* **2000**, *50*, 173–184.
(34) Morell, J., M.; Capella, J.; Mercado, A.; Bauza, J.; Corredor, J. E. Nitrous oxide fluxes in Caribbean and tropical Atlantic waters: Evidence for near surface production. *Mar. Chem.* **2001**, *74*, 131–143.

(35) Bange, H. W.; Naik, H.; Naqvi, S. W. A. Enhancement of oceanic nitrous oxide emissions by storms. *Solas News* December, **2008**, *8*, 9.
(36) Nevison, C. D. ; Lueker, T. J.; Weiss, R. F. Quantifying the nitrous oxide source from coastal upwelling. *Global Biogeochem. Cycles* **2004**, *18*, DOI: 10.1029/2003GB002110.
(37) Diaz, R. J.; Rosenberg, R. Spreading dead zones and consequences for marine ecosystems. *Science* **2008**, *321*, 926–929.
(38) Webster, P. J.; Holland, G. J.; Curry, J. A.; Chang, H. R. Changes in tropical cyclone number, duration, and intensity in a warming environment. *Science* **2005**, *309*, 1844–1846.
(39) Landsea, C. W.; Harper, B. A.; Hoarau, K.; Knaff, J. A. Can we detect trends in extreme tropical cyclones. *Science* **2006**, *313*, 452–454.

ES902058T